Journal of Statistical Physics, Vol. 93, Nos. 3/4, 1998

On Spherically Symmetric Gravitational Collapse

Michael P. Brenner[1] and Thomas P. Witelski[1, 2]

Received February 5, 1998; final July 27, 1998

This paper considers the dynamics of a classical problem in astrophysics, the behavior of spherically symmetric gravitational collapse starting from a uniform, density cloud of interstellar gas. Previous work on this problem proposed a universal self-similar solution for the collapse yielding a collapsed mass much smaller than the mass contained in the initial cloud. This paper demonstrates the existence of a second threshold—not far above the marginal collapse threshold—above which the asymptotic collapse is not universal. In this regime, small changes in the initial data or weak stochastic forcing leads to qualitatively different collapse dynamics. In the absence of instabilities, a progressing wave solution yields a collapsed uniform core with infinite density. Under some conditions the instabilities ultimately lead to the well-known self-similar dynamics. However, other instabilities can cause the density profile to become non-monotone and produce a shock in the velocity. In presenting these results, we outline pitfalls of numerical schemes that can arise when computing collapse.

KEY WORDS: Gravitational collapse; singularities in nonlinear partial differential equations; self-similar solutions.

1. INTRODUCTION

Singularity formation in nonlinear partial differential equations is a topic of current interest,[(1)] about which both authors have learned a great deal from Leo Kadanoff, both directly (MB) and indirectly (TW). The present contribution to this volume discusses gravitational collapse, a classical problem in astrophysics that shares an important feature with problems that Kadanoff has recently studied (see, e.g., ref. 2), in that there is presently believed to be a "universal similarity solution" (in this case discovered by

[1] Department of Mathematics, Massachusetts Institute of Technology, Cambridge, Massachusetts 02139-4307.

[2] Present address: Department of Mathematics, Duke University, Durham, North Carolina.

0022-4715/98/1100-0863$15.00/0

Larson[3]) to which a large class of initial data converge. However, gravitational collapse differs from these examples in that it produces singularities without dissipation. Without dissipation there is no a priori guarantee for a (finite) basin of attraction for a "universal" singularity. This study demonstrates that this problem contains a nonlinear threshold, above which the asymptotic form of the collapse singularity is not universal: in this regime slight changes in the initial data—or the presence of a small stochastic noise source—can lead to convergence to (at least) three possible asymptotic solutions near the singularity. One of the solutions was known previously for marginally unstable collapse[3] and was thought to be universal. Whether this sensitive dependence on initial data represents a general property of singularity formation in nondissipative systems[4] is an interesting question.

Gravitational collapse has been examined extensively in astrophysics as a possible mechanism for the formation of planets and stars. A recent example is the work of Boss on the formation of giant planets.[5] Three-dimensional hydrodynamic equations were solved numerically starting from an initial spinning disk of gas, and it was found that the evolution leads to spiral density waves, in which there eventually form singularities in the material density. The idea that this might represent a mechanism of planet formation dates back at least to Kuiper.[6] Boss argues that in his simulations the mass of these planets was of the order of magnitude of the masses of "giant planets" like Jupiter[7] and that therefore gravitational instability is a possible formation mechanism. A competing idea for the formation of giant planets, operating on a much slower timescale, is the gradual accumulation of mass over long periods of time.[8] This divergence of views for the mechanisms of planet formation reflects both the intrinsic complexity in the dynamical equations governing three-dimensional gravitational collapse, as well as the large range of timescales over which the observable system has evolved. Astrophysical overviews can be found in refs. 9–11. Studies in statistical physics have also addressed the nature of gravitational collapse for systems of particles.[12]

A basic question of gravitational collapse is to determine the distribution of mass and the formation of singularities starting from a uniform density initial state. In 1969 Larson[3] proposed studying the simplified problem of gravitational collapse with *spherically symmetric* dynamics and quiescent isothermal uniform density initial conditions. Although the relationship of this problem to the full problem is unclear, it allows both numerical and semi-analytical progress regarding the different stages of collapse. Larson solved the compressible Euler equations, supplemented by radiation, heat transfer and chemical reactions for a marginally unstable spherically symmetry cloud of one solar mass, and developed a unified

scenario for the different stages of the collapse which he identified as the precursor of star formation. In the earliest stage, for material densities approximately between 10^{-19} g/cm^3 and 10^{-13} g/cm^3, the collapse is isothermal and is described by the compressible Euler equations with an isothermal equation of state. For these equations, there is a similarity solution which describes the formation of a singularity of the material density. This similarity solution was discovered independently by Penston,[13] and is called the Larson–Penston solution; the discovery of this solution led researchers to believe that all gravitational collapse singularities occur in a self-similar way with the universal features that (a) the farfield velocity field approaches the uniform constant value $u \sim -3.3c$ where c is the speed of sound in the homogeneous gas, and (b) the density decays algebraically of the form $\rho \sim 8.9r^{-2}$ as $r \to \infty$. This solution also predicts that the mass involved in the initial collapse is much smaller than the mass of the cloud.

The universality of the Larson–Penston solution was criticized by Shu,[14] who pointed out that it was the solution of a very specific boundary value problem that was not representative of initial conditions expected in most situations. In particular, Shu argued that it is necessary for the boundary conditions on the cloud to have the far-field infall velocity of $-3.3c$. Namely that far from the center of the cloud all of the mass experiences a uniform inward velocity of 3.3 times the speed of sound. As an alternative scenario, Shu proposed that the relevant physical problem is the determination of the flow following the formation of a core with a small mass. With this modification, he demonstrated that there is a one parameter family of similarity solutions governing the collapse so there can be a continuous dependence of the infall velocity on ρ_0. Although this solution circumvents the difficulty of a universal infall velocity, it has the unsatisfactory feature that it assumes the existence of an initial core, without addressing its formation mechanism.[15] Subsequent numerical simulations[16, 17] have demonstrated that the far-field limit of the infall velocity, to $u \sim -3.3c$ is established dynamically during the collapse process. Gravitational collapse is an example of the formation of a localized singularity; as the collapse time is approached the lengthscale describing the region of the collapse becomes vanishingly small. Thus, as the collapse proceeds, the far-field of the solutions occurs not far from the collapse point in absolute distances. In terms of matched asymptotic expansions, the collapse dynamics describe an inner solution that must connect to a slowly varying outer solution describing the remainder of the interstellar cloud. Another aspect of Shu's criticism is more difficult to dismiss: consider the collapse dynamics in a spherical cloud of constant radius with increasing initial density ρ_0. At very small ρ_0, pressure overwhelms gravitational attraction so collapse does not occur. At a critical density, the cloud will collapse, and

form a singularity. Upon increasing the initial density ρ_0 far above the critical density, the collapse becomes more violent. Eventually, the infall velocity will exceed $-3.3c$. This argument suggests that far above the collapse threshold, the infall velocity should somehow depend on ρ_0. The strange feature of positing the Larson–Penston solution as a "universal" collapse dynamic is that it means that the final value of the infall velocity is independent of ρ_0.

The primary goal of this paper is to resolve this issue by presenting a detailed analysis of the collapse dynamics of a spherical cloud as a function of its initial density ρ_0. At sufficiently low density, thermal pressure is more important than self gravitation and the cloud does not collapse. Beyond a certain first threshold for the initial density, collapse occurs. At intermediate densities the asymptotic dynamics is described by the Larson–Penston solution. The mass contained in the resulting collapsed region is orders of magnitude smaller than the mass of the total cloud. We demonstrate the existence of a second threshold for the initial density, above which the collapse dynamics qualitatively changes. This threshold occurs when the free fall time for a particle at the edge of the cloud is shorter than the time for sound wave propagation across the cloud. In this regime, collapse to infinite density occurs in the center of the cloud *before* density inhomogeneities can propagate into the center of the cloud. In contrast to the Larson–Penston solution, the resulting collapsed region has a finite mass, on the order of the total mass in the cloud.

However, the uniform density core of this collapsing solution is dynamically unstable to a Jeans-like instability; before complete collapse occurs there can be a transition to another behavior. From numerical simulations we demonstrate at least three possible outcomes: either the solution collapses to infinite density and infinite infall velocity with a spatially uniform core; the solution converges onto the Larson–Penston solution (in which, as above, an extremely small percentage of the total cloud mass contributes to the ultimate collapse) and has a finite infall velocity; *or* the density profile becomes nonmonotonic, and develops a shock in the velocity which propagates towards the center of the cloud. This first and third scenarios appear to be novel mechanisms for spherically symmetric collapse. Taken together, our results present a unified picture of how the collapse dynamics changes with increasing material density in the cloud, and provides an alternative resolution to Shu's criticism, in which it is unnecessary to assume an initially static core.

This paper is organized as follows: Section 2 describes two different formulations of the initial value problem, and introduces the dimensionless parameter describing the initial data. Section 3 then demonstrates the existence of the nonlinear threshold described above, and gives the uniform-core

solution describing the collapse above this threshold. Numerical simulations as a function of the governing parameter are presented. Above a critical value it is demonstrated that either spatial nonuniformities in the initial data *or* small fluctuations in the force balance can destabilize the uniform-core solution. Two types of subsequent dynamics are distinguished, depending whether the density profiles are monotonic or nonmonotonic. Section 4 discusses similarity solutions, and focuses on the asymptotics of the collapse near the singularity. Section 5 describes subtleties in designing numerical algorithms for capturing the collapse, including the existence of rather subtle spurious numerical solutions to the equations. The appendix describes additional properties of the equations that are useful for interpreting our results.

2. GOVERNING EQUATIONS

In this section we use the equations governing gravitational collapse of a compressible inviscid fluid to formulate the problem of the formation of a protostar from a cloud of interstellar molecular gas. The governing equations for the conservation of mass and momentum, and the gravitational potential are

$$\rho_t + \nabla \cdot (\rho \mathbf{v}) = 0 \tag{1}$$

$$\rho(\mathbf{v}_t + \mathbf{v} \cdot \nabla \mathbf{v}) = -\nabla p + \rho \nabla \phi \tag{2}$$

$$\nabla^2 \phi = -4\pi G \rho \tag{3}$$

where ρ is the density, $\mathbf{v}$ is the velocity, ϕ is the gravitational potential, p is the pressure field and $G \approx 6.67 \times 10^{-11}\ \mathrm{Nm^2/kg^2}$ is Newton's gravitational constant. The pressure is determined by the heat transfer conditions. During the collapse, the gas will be heated by compressional heating, and cooled by radiation. It is commonly assumed[3] that the net result of the heat transfer is that the gas is isothermal until the densities are high enough that the core is optically thick. We will follow this assumption herein, and consider an isothermal equation of state $p = c^2 \rho$, where c is the speed of sound in the initial uniform quiescent interstellar gas.

If the size of the cloud is sufficiently large it will collapse. The collapse results in a clumping singularity, in which the material density diverges at the origin in finite time. A rough estimate for the critical size of the cloud can be computed by linear stability analysis of equations (1)–(3) in unbounded space; perturbations of a uniform, infinitely extended fluid grow if their characteristic wavelength is larger than the Jeans[18] wavelength $\lambda_J = 2\pi c/\sqrt{4\pi G \rho_0}$, where ρ_0 is the initial density. Clouds with radii

much larger than the Jeans length will typically fragment into a number of different regions, in which the material density is rapidly growing. A fundamental question (which to our knowledge has not yet been fully answered) is to understand the final mass distribution and formation of singularities that results from this dynamics, and how the distribution depends on the initial size, shape and density of the cloud. Answering this question requires considering the dynamics of a fully three-dimensional collapse; observations[19] suggest there may be transient structures of more complicated geometries intermediate between the initial constant density regime and the final state consisting of spherical point masses. A statistical mechanical study has revealed that in a finite closed system, the free energy minimum consists of concentrated point masses.[12]

The issue addressed in this paper is to determine the nature of the dynamics when spherical symmetry is enforced and the initial density of the cloud is constant, as in Larson's original work. This model can be hoped to serve as a good description of the intermediate asymptotics during gravitational collapse. In the final stages of collapse, when very large densities have been achieved, it is clear that many assumptions used to write (1)–(3) will no longer hold. Similarly, many complications that could be expected from realistic velocity fields and initial conditions have been neglected. In solving this problem we assume that the idealized system is capable of capturing some of the qualitative properties and parametric dependencies, even if complications such as radiation effects, non-isothermality, angular momentum and general relativity will modify some quantitative results.

In light of this, the present study will examine the nature of the collapse as function of the effective initial density of the cloud, without regard to how far the cloud is from equilibrium. We consider a spherical cloud of radius $\mathscr{R}_c$ with initially uniform density ρ_0. There is a single dimensionless parameter that describes the dynamics,

$$N \equiv \frac{4\pi\rho_0 \mathscr{R}_c^2 G}{c^2} = \frac{1}{\mathrm{Fr}^2} = \left(\frac{\mathscr{R}_c}{\mathscr{R}_J}\right)^2 \tag{4}$$

This parameter is equal to the square of the ratio of the cloud radius to the Jeans length $\mathscr{R}_J = c/\sqrt{4\pi G\rho_0}$. N can be expressed as one over the square of the Froude number, $\mathrm{Fr} = \mathscr{R}_J/\mathscr{R}_c$, which represents the ratio of pressure to gravity effects. The central goal of this paper is to describe the nature of the collapse in terms of N.

We nondimensionalize the equations (1)–(3) by scaling densities in terms of ρ_0, lengths by the cloud radius $\mathscr{R}_c$, and timescales in terms of

$\mathscr{R}_c/c$. In dimensionless units, the spherically symmetric equations of motion become

$$\rho_t + \frac{1}{r^2}(r^2\rho u)_r = 0 \tag{5}$$

$$u_t + uu_r + \frac{\rho_r}{\rho} - N\phi_r = 0 \tag{6}$$

$$\frac{1}{r^2}(r^2\phi_r)_r + \rho = 0 \tag{7}$$

An important property of equations (5)–(7) is that they are hyperbolic. Despite the elliptic Poisson equation (7) for the gravitational potential, the overall system of equations can be expressed in terms of Riemann variables evolving on characteristics.[20] The properties of similar gas dynamic models have been extensively studied in relation to shocks and spherical waves[21–23] and the isothermal model.[24] The Riemann variables for this system are

$$\alpha(r, t) = \ln(\rho) + u, \qquad \beta(r, t) = \ln(\rho) - u \tag{8}$$

corresponding to the evolution equations on the characteristics

$$\frac{d\alpha}{dt} + \frac{2}{r}u - Nf = 0 \quad \text{on} \quad C_+ : \frac{dr}{dt} = u + 1 \tag{9}$$

$$\frac{d\beta}{dt} + \frac{2}{r}u + Nf = 0 \quad \text{on} \quad C_- : \frac{dr}{dt} = u - 1 \tag{10}$$

where the gravitational force $f = \phi_r$ is given by

$$\frac{df}{dr} + \frac{2}{r}f + \rho = 0 \rightarrow f = -\frac{1}{r^2}\int_0^r \rho(\tilde{r}, t)\,\tilde{r}^2\,d\tilde{r} \tag{11}$$

defined for each instant in time. The characteristic equations (9), (10) form a timelike coupled system, while the characteristic (11) defining the gravitational force is space-like and decoupled. In most studies of gravitational collapse the gas cloud is initially taken to be at rest or near equilibrium. When the velocity u is small, the C_+ characteristics propagate outward (9), while the C_- characteristics propagate toward the origin (10). Under conditions where collapse occurs, the material infall velocity can become large and negative. In regions of space where the flow is supersonic, $u < -1$, both families of characteristics carry information toward the origin. The

hyperbolicity of this problem is an important feature in the calculations presented herein, both in establishing several important exact relations about the collapse, and in formulating and assessing the reliability of numerical schemes for solving the equations.

3. STAGES OF THE COLLAPSE

This section describes the various regimes of behavior which occur during gravitational collapse of a finite mass, finite size gas cloud in otherwise empty, unbounded space. For N below a critical value, gravitational forces are not large enough to overcome pressure, and collapse does not occur. The collapse threshold occurs roughly when the cloud radius is of order the Jeans wavelength. The opposite limit ($N \to \infty$) corresponds to a cloud with finite initial density but infinite extent. In this case, the material density increases in time but (in the absence of external perturbations) remains spatially uniform within a core region in the interior of the cloud throughout the collapse (see Fig. 1). Spatial uniformity within this central core can only broken by the growth of small perturbations due to inhomogeneities or external forcing. As the material density increases, the characteristic Jeans scale where nonuniformity can occur decreases. At a finite N, there are two distinct mechanisms for generating spatial nonuniformity in the center of the cloud: first, in the $N \to \infty$ limit, spatial perturbations to the constant density core tend to grow; secondly, the boundary conditions at the edge of the cloud causes a density gradient to form, which propagates in towards the origin.

Many earlier studies have considered the problem of a self-gravitating cloud contained within a fixed finite region of space with no-flux boundary conditions at the edges of the domain.[3, 17, 16] We will show that the details of gravitational collapse do not depend on the nature of the far-field boundary conditions. Consequently, we consider the slightly more realistic problem of a finite self-gravitating cloud released in free space. For the purpose of computations, our numerical simulations describe a cloud of interstellar gas starting from rest with an initially uniform density on a finite region, $0 \leqslant r \leqslant 1$, with either an absorbing or a no-flux boundary condition at $r = 1$. The results of these simulations describe the interior, $0 \leqslant r \ll 1$, of a self-gravitating cloud in unbounded space, $0 \leqslant r < \infty$, when waves reflected from $r = 1$ are neglected. As will be discussed further, the nature of the far-field boundary condition will not qualitatively change many properties of the collapse behavior, as has been shown in other studies using various boundary conditions at the edge of the cloud.[17] This property is a consequence of the nature of the collapse forming a spatially localized singularity that will ultimately be independent of the far-field behavior in the problem.

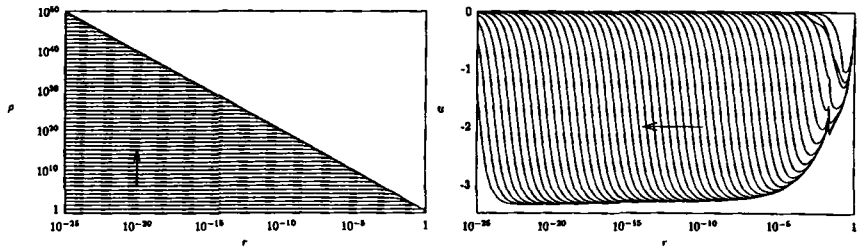

Fig. 1. Full numerical simulation of the gravitational collapse for $N = 10$. The simulation was halted shortly before the formation of the singularity, when the density at the origin reached $\rho \approx 10^{50}$. As will be discussed later, following the initial transient behavior, the solution follows a self-similar evolution.

A representative example of the dynamics above the marginal collapse threshold ($N = 10$) is given in Figs. 1 and 2. The initially uniform cloud rapidly develops a central core of increasing density. As the critical collapse time, when infinite density is achieved, $t \to t_c$ is approached the density increases, the core radius decreases and the lengthscale of the solution decreases. This behavior makes it convenient to plot ρ and u on logarithmic scales. Figure 1 shows that the density profile obeys $\rho \sim r^{-2}$ away from the high density core, and the velocity asymptotes to a constant near -3.3 times the sound velocity.

3.1. The Constant Density Core

To understand the numerical solutions it is useful to first develop a theory for the dynamics of the constant density "core" region of the gas cloud. Our aim is to both provide a more complete picture of the dynamics as a function of N, and to derive a formula for how the amount of mass that eventually collapses depends on the properties of the initial cloud, N.

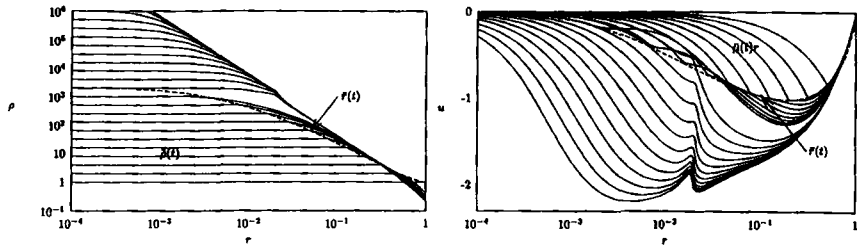

Fig. 2. Numerical simulation of the initial stages of gravitational collapse for $N = 10$. The envelope showing the edge of the uniform density region $\bar{r}(t)$ (See Subsection 3.1) is shown with dashed lines. At $N = 10 < N_C$ the radius of the uniform core vanishes when $\rho \approx 2200$.

Initially it is assumed that the entire cloud is at rest with constant density. The conditions at the edge of the cloud break the uniformity of the density. As the collapse progress, the region of uniform density contracts to a smaller and smaller portion of the cloud, with the radius being determined by the region of influence of the cloud boundary; this is a direct consequence of the hyperbolicity of the equations. We will see below that understanding the dynamics of this uniform density region is critical to understanding how much of the mass of the cloud collapses to a point. The mathematics of our analysis generalizes previous work of Hunter,[16] though our point of view is different: whereas he considered the constant density solution as the leading term in a Taylor series expansion about the origin, we claim that the constant density region holds exactly in a finite region surrounding the origin for a period of time. The constant density solution takes the form

$$\rho(r, t) = \bar{\rho}(t), \qquad u(r, t) = \bar{\mu}(t)\, r \tag{12}$$

Substituting into (5)–(7) yields

$$\frac{d\bar{\rho}}{dt} = -3\bar{\rho}\bar{\mu}, \qquad \frac{d\bar{\mu}}{dt} = -\frac{N}{3}\bar{\rho} - \bar{\mu}^2 \tag{13}$$

This system exactly describes a large neighborhood of the origin when spatial gradients have not propagated in from the edge of the cloud. We remark that since the density is assumed uniform in the core of the cloud, the pressure gradient term in (6) is absent in (13); this is sometimes called a homologous collapse or is described as free-fall behavior. It is clear from these equations that both the density and the magnitude of the velocity gradient will monotonely increase in time. System (13) can be solved implicitly for a cloud with initial density $\bar{\rho} = 1$ at rest with initial velocity $\bar{\mu} = 0$. The uniform core density and velocity gradient are given implicitly by

$$\begin{aligned} t &= \sqrt{\frac{3}{2N}}\left(\frac{1}{\bar{\rho}^{1/3}}\sqrt{\bar{\rho}^{1/3} - 1} + \arctan\sqrt{\bar{\rho}^{1/3} - 1}\right) \\ \bar{\mu} &= -\sqrt{\frac{2N}{3}\bar{\rho}(1 - \bar{\rho}^{-1/3})} \end{aligned} \tag{14}$$

A formula for the radius of the uniform density region follows from examining the propagation of the influence of the edge of the cloud. In our numerical simulations, the influence of the outer boundary conditions is equivalent to assuming some sharp profile for the transition between $\rho = 1$

and $\rho \to 0$ outside the cloud. Solving a spherical Riemann problem at the edge of the cloud would yield possible contact discontinuities and shocks propagating outward; these waves will not influence the dynamics of the collapse and can be neglected for our purposes. In studies where the cloud is held within a finite container, these outgoing waves will be reflected and can lead to convergence to the Emden equilibrium gas sphere solution.[25] The velocity "rarefaction wave"[22] propagating toward the origin, and its reflection from the origin determine the dynamics of collapse. Since the equations (5)–(7) are hyperbolic, the influence of the edge of the cloud moves at the velocity of the fastest inward characteristic,[20] C_- (10), given by

$$\frac{d\bar{r}}{dt} = \bar{\mu}\bar{r} - 1, \qquad \bar{r}(0) = 1 \tag{15}$$

Using (14) yields a relation between the core radius and the density,

$$\bar{r} = \frac{1}{\bar{\rho}^{1/3}}\left(1 - \sqrt{\frac{6}{N}} \arctan \sqrt{\bar{\rho}^{1/3} - 1}\right) \tag{16}$$

The hyperbolicity of the dynamical equations implies that for radii less than $\bar{r}$, the density profile remains spatially uniform, $\rho = \bar{\rho}(t)$ for $r \leqslant \bar{r}(t)$.

To determine the final state resulting from the evolution of the uniform core we determine $\bar{t}_f$ time to when the radius of the uniform density region vanishes, $\bar{r}(\bar{\rho}_f) = 0$, to yield

$$\bar{\rho}_f = \sec^6\left(\sqrt{\frac{N}{6}}\right), \qquad \bar{t}_f = \frac{1}{2}\left(1 + \sqrt{\frac{3}{2N}} \sin \sqrt{\frac{2N}{3}}\right), \qquad N < \frac{3\pi^2}{2} \tag{17}$$

$$\bar{\rho}_f = \infty, \qquad \bar{t}_f = \frac{\pi}{2}\sqrt{\frac{3}{2N}}, \qquad N \geqslant \frac{3\pi^2}{2} \tag{18}$$

For $N < N_C \equiv 3\pi^2/2 \approx 14.8$ the final core density will be finite at the time of collapse, while for $N > N_C$, $\bar{\rho}$ becomes infinite simultaneously as the core collapses $\bar{r} \to 0$ at time $\bar{t}_f$. The above results can be combined to determine the mass of the core, $\bar{M} = 4\pi\bar{\rho}\bar{r}^3/3$. The mass is related to the density by

$$\frac{d\bar{M}}{d\bar{\rho}} = \frac{4\pi\bar{r}^2}{3\bar{\mu}}, \qquad \bar{M}(\bar{\rho} = 1) = \frac{4\pi}{3} \tag{19}$$

For $0 < N < 3\pi^2/2$, the mass of the uniform core vanishes when the radius of the core region goes to zero since the density is finite, $\bar{M}_f = 4\pi\bar{\rho}_f\bar{r}_f^3 \to 0$.

When $\bar{\rho} \to \infty$ the radius of the core (16) also vanishes. Using this limit in the solution of (19), we observe that the core collapses to a point with finite mass for $N > N_C$,

$$\bar{M}_f = \frac{4\pi}{3}\left(1 - \pi\sqrt{\frac{3}{2N}}\right)^3 \tag{20}$$

This formula shows that for $N = 3\pi^2/2$ the collapsed core has zero mass, while in the limit $N \to \infty$ the core will include the entire mass of the gas cloud. Hence, in the absence of external perturbations to the uniform density region, when $N > N_C$ the cloud collapses to a spatial point of infinite density, with a mass given by equation (20).

Note that spatial nonuniformities or dissipative effects can effectively reduce the size of the uniform core region; if the onset of nonuniformities begins at $r = f < 1$ then $N_{\text{eff}} \approx f^2 N < N$. A consequence of this is that the critical value $N_C = 3\pi^2/2$ can be increased by various factors; numerical schemes that introduce dissipation, inhomogeneous initial conditions, and numerous physical effects.

The following subsection examines the dynamics just above the marginal collapse threshold more closely, and illustrates the delicate competition between gravity and pressure waves which try to halt the collapse. Then, we will turn to $N > N_C$, and present numerical simulations which show the influence of spatial gradients from the edge of the gas cloud and the accompanying pressure effects *can not* prevent the formation of a uniform infinite density core region. In the absence of other perturbations, this uniform density solution provides an exact description of the collapse. However, this solution is generically unstable, so that if perturbations to the density field exist, the collapse develops further spatial structure and the dynamics follows a different collapse mechanism.

3.2. The Threshold for Collapse

While the above description of the dynamics of the uniform core applies for all values of N, there is a certain minimum value $N_M < N_C$ below which the evolution after $\bar{t}_f$ disperses the cloud rather than collapsing it. If the initial cloud radius is small, $\mathcal{R}_c \ll \mathcal{R}_J$, then collapse will not occur. Collapse occurs roughly when $\mathcal{R}_c \sim \mathcal{R}_J$ and gravitational attraction can overcome pressure effects. A precise threshold follows from examining stationary hydrostatic solutions of equations (5)–(7), which obey the Liouville or Lane–Emden equation,[25–29]

$$\nabla^2 \ln \rho = -N\rho \tag{21}$$

This equation also arises in bacterial chemotaxis.[30, 31] The far-field asymptotics, $r \to \infty$, for these stationary solutions are given by refs. 25, 16, 26, 31

$$\rho_s(r) \sim \frac{2}{Nr^2} \exp\left(\frac{A \cos[\sqrt{7/4}\ln(r)]}{\sqrt{r}}\right) \tag{22}$$

We note in particular that the mass $M = 4\pi \int \rho r^2\, dr$ of these solutions is infinite for an isolated cloud in free space. Consequently, there is no threshold value for N based on equilibrium solutions for finite mass clouds in unbounded domains. Clouds that do not eventually collapse can expand indefinitely. On the other hand, for systems in bounded domains the situation is different: Equilibrium solutions with finite mass exist, and have been well studied, starting with the pioneering work of Emden (see references in 12, 29, 25). It should also be remarked that stationary solutions on a bounded domain are also relevant for the dynamics in unbounded space as long as the timescale of interest is much shorter than the time for absence of the boundary to affect the dynamics inside the cloud.

M. Kiessling[32] has pointed out to us (private communication) the interesting history associated with Emden's contributions to this subject, which are contained in Emden's 1907 book.[25] The book contains both a thorough discussion not only of the properties of the equilibrium solutions in free space, but also, an entire chapter called "Gas balls in rigid confinement" on the solutions in a finite region. Emden's central result is that below a critical dimensionless temperature 0.39688, no equilibrium solutions to the equation in a finite box exist. In the present language, since N is inversely proportional to temperature, this turns out to correspond to a maximum $N = 3 \times (0.39688)^{-1} \approx 7.5$, where the factor of 3 arises from different notations.[3] The existence of a critical N in these equations in three dimensions has been subsequently rediscovered many times in different contexts (e.g., ref. 31). As a historical note, Kiessling also pointed out to us that although Emden's book is not available in English translation, the

[3] Emden's 1907 calculation of this number to five significant digits is a remarkable feat, considering that it requires accurately integrating a second order nonlinear ordinary differential equation. Mathematica gives a critical temperature of 0.3972, which means that Emden's calculation is correct to 3 significant figures! Emden's acknowledgements of help with this calculation are particularly interesting: he states "... I still have the pleasant duty to thank my students for carrying out a large part of the ensuing mechanical quadratures; my colleague Mr. Dr. W. Kutta, whose approximation scheme was thereby applied, for his practical advice, and for his communications on p. 92–95, in which the precision of the method and its applications to differential equations of second order is explained; and last but not least Mr. Prof. K. Schwarzshild in Göttingen,..." (Translation by M. Kiessling).

"classical" part of Chandrasekhar's book[26] is based on the first ten chapters of Emden's book. The discussion on confined gases is contained in Emden's Chapter 11.

Our computer simulations of the dynamics allow us to estimate a lower value of approximately $N_M \approx 6.6$, in agreement with Larson's value of $N_M \approx 6.52$.[3] For $N < N_M$, pressure effects ultimately dominate over gravity and a strong pressure wave reflects from the origin, increasing the local velocity (see Fig. 3). At intermediate times before this outward wave reaches the boundary of the cloud, the local density profile near the origin closely resembles the structure of a quasistatic Emden solution of (21),

$$\tilde{\rho}_s(r, t) \sim \rho_0 - \frac{N\rho_0^2}{6} r^2 + \cdots \tag{23}$$

where $\rho_0 = \rho_0(t)$ is slowly varying function of time that gives the density at the origin. For longer times, the density $\rho_0(t)$ will decrease with time and yield deviations from the Emden solution, as determined by the influence of the far-field boundary conditions. In particular, in unbouned space, where there is no finite mass stationary solution, the cloud would then completely dissipate.

To understand the significance of the critical value $N_M \approx 6.6$, it is important to note that it is a nonlinear dynamic threshold. Below this value, dynamically generated pressure waves can balance the effects of gravitational attraction and prevent collapse. In a finite spherical geometry, the critical value of $N_E \approx 7.5$ mentioned above is derived from the conditions needed for the existence of an non-collapsed equilibrium solution. A linearly stable Lane–Emden solution exists for each $N < 7.5$ and should be an attractor of the dynamics for initial conditions sufficiently close to it.[12, 33, 34] The fact that we have calculated collapse occuring for

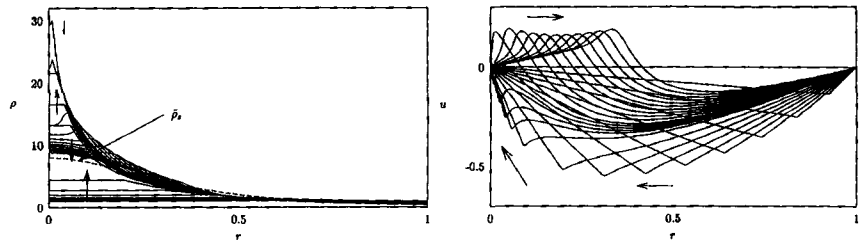

Fig. 3. Numerical simulation of the initial dynamics below threshold for $N = 6$. Initially the velocity becomes negative, $u < 0$, and the density increases at the origin under free-fall. However, eventually, the influence of the cloud boundary reaches the origin and produces a reflected pressure wave with $u > 0$, causing mass to spread out and density to decrease. The density profile resembles a slowly-varying equilibrium solution $\tilde{\rho}_s(r; t)$.

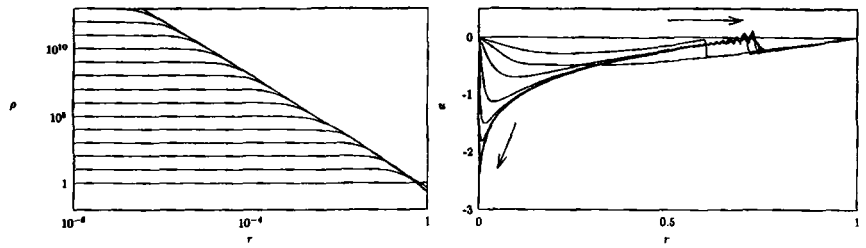

Fig. 4. Numerical simulation of the initial dynamics for the cloud slightly above threshold at $N = 6.75 > N_M$. Gravitational collapse occurs as $\rho \to \infty$ and the velocity remains negative near the origin, $u \leqslant 0$. The reflected pressure wave steepens and forms a shock (yielding minor oscillatory instabilities in the numerical scheme) as it propagates outward.

$N_M < N < N_E$ suggests that the Emden equilibrium solution is not a global attractor, and the uniform density initial state is far from equilibrium.

Indeed, Kiessling[12] also proved that there is a distributional stationary solution, corresponding to a collapsed state, that minimizes the free energy, co-existing in the same regime as the linearly stable Emden solution. Hence, at thermodynamic equilibrium, his argument suggests that the preferred configuration is the completely collapsed cloud. The implication of this theorem is that for all finite $N < 7.5$ the linearly stable Emden solutions are merely metastable, separated by a free energy barrier from the preferred completely collapsed state.[4] The significance of our number $N = 6.6$ is that it characterizes the initial condition on the borderline between the basins of attraction of the collapsed state and the regular stationary solution. When $N > 6.6$, the free energy of the initial condition is sufficient to overcome the "barrier" that surrounds the metastable Emden solution.

For $N > N_M$, while there is still a reflected pressure wave, it is not strong enough to overcome the gravitational collapse; the velocity near the origin remains negative while the local density diverges, $\rho \to \infty$ in finite time. Note that the outgoing pressure wave steepens as it propagates, and in Fig. 4 it has formed a velocity shock. The details of this shock at a finite distance from the origin do not influence the localized structure of the singularity. As N increases, gravity becomes more important and the reflected pressure wave has a smaller and smaller effect. This trend is illustrated in Fig. 5, which shows the velocity profiles close to the critical time for a

[4] We note that Kiessling's theorem states that the preferred state has all of the mass in the system collapsed at the origin; our calculations do not follow the collapse this far when N is low, as in this regime, the initial collapse only concentrates a very small fraction of the total mass of the cloud, as discussed above. Presumably, (in spherical symmetry) the dynamics after the first collapse will eventually lead to all of the mass collecting at the origin.

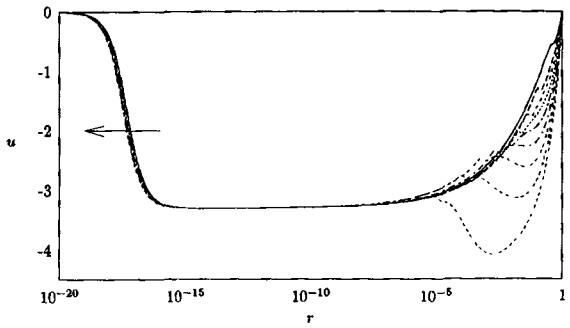

Fig. 5. Comparison of the velocity fields $u(r, t)$ at $N = 7, 8, \ldots, 14, 15$ very close to their respective critical times. Initial behavior shows distinct transient wave interactions, but independent of N, all cases converge to the same solution for $t \to t_c$.

range of N between N_M and N_C. The initial dynamics, at finite length scales, show various transient responses, while as the collapse time is approached, all of the solutions converge to the same velocity profile at small lengthscales. This is the Larson–Penston similarity solution.

Another indicator of the influence of pressure on the collapse is the collapse time, t_c. In the absence of pressure, the collapse time would be equal to the free fall time for matter to fall from the outside of the cloud to the center. Figure 6 shows a comparison of the collapse time t_c obtained from numerical simulations and the free-fall time $\bar{t}_f$ (17), (18). For $N < N_M$ no collapse occurs, but the free-fall time is finite. On the interval $N_M \leqslant N < N_C$, $\bar{t}_f$ underestimates the collapse time t_c; below N_C, free-fall behavior ends at $\bar{t}_f$ with a finite density at the origin, then further dynamics must follow to yield the collapse, $\rho \to \infty$. For $N > N_C$, $\bar{t}_f$ is a very good estimate of the collapse time, but as we will describe below it is an upper bound,

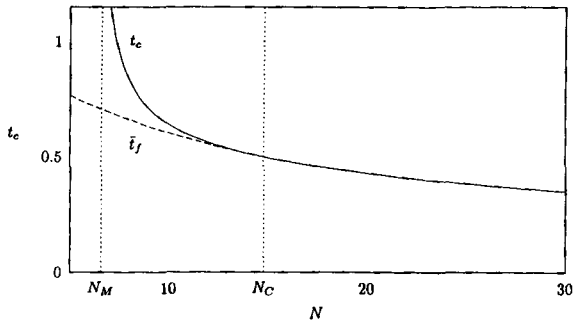

Fig. 6. Comparison of the free-fall time $\bar{t}_f$ (17), (18) with the collapse time t_c obtained from numerical simulations over a range of different values for N.

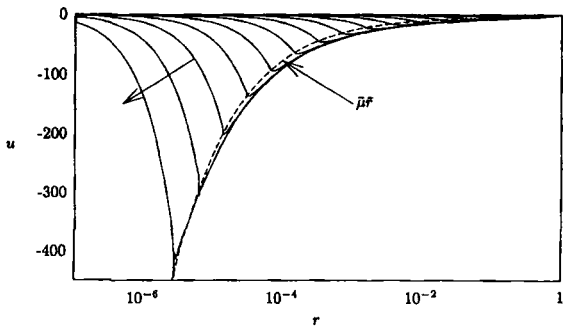

Fig. 7. In contrast to the subcritical case, for $N = 30 > N_C$, the velocity does not necessarily saturate, and can grow indefinitely (in the absence of instabilities). The dashed line represents the constant density solution. Errors due to limitations in the numerical scheme begin to become apparent in the last profile.

because instabilities to the uniform core solution will hasten the collapse. Finally, we note that slightly above N_M, the collapse time obeys a singular power law, $t_c \sim (N - N_M)^{-0.3}$. Larson's original simulations[3] were done not far above threshold, at $N \approx 7.3$.

3.3. Instability of Uniform Density Supercritical Collapse

For $N > N_C$, the uniform core solution describes that *both* the density of the core and the maximum gas velocity becomes infinite at some finite critical time t_c. This is demonstrated in a numerical simulation in Fig. 7, which shows the velocity becoming very large and negative for $N = 30$.

However, we expect the dynamics of,the collapse to deviate from a uniform core. one cause is nonuniformity in the initial conditions. Another is that even for perfectly uniform initial conditions, the uniform density state is unstable against small fluctuations. One can see this qualitatively by noting that the Jeans scale $2\pi/\sqrt{\rho N} \sim (t_c - t)$ is asymptotically smaller than the radius of the uniform density region, which is of order $(t_c - t)^{2/3}$.

To demonstrate the instability of the uniform core, we study the evolution of small perturbations to the uniform density solution constructed above. Since we are interested in the dynamics close to the collapse, it is convenient to use the asymptotics of the uniform solution (14), (16) in the limit that $\rho \to \infty$

$$\bar{\rho} \sim \frac{2}{3N}\tau^{-2}, \qquad \bar{\mu} \sim -\frac{2}{3}\tau^{-1}, \qquad \bar{r} \sim \left(\frac{3N}{2}\right)^{1/3}\left(1 - \pi\sqrt{\frac{3}{2N}}\right)\tau^{2/3} \tag{24}$$

where the time to collapse is $\tau = t_c - t$ and the critical time is

$$t_c = \frac{\pi}{2}\sqrt{\frac{3}{2N}} \tag{25}$$

To compute the stability of the spatially uniform solution for $0 \leqslant r < \bar{r}(t)$ as $t \to t_c$, we consider the following perturbations to the core

$$\rho = \bar{\rho}(t)(1 + \mathscr{R}(\xi, s)), \qquad u = \bar{\mu}(t)\, r + \tau^{-1/3}\mathscr{U}(\xi, s) \tag{26}$$

where the independent variables for the perturbation are

$$\xi = \frac{r}{\tau^{2/3}}, \qquad s = -\ln(\tau) \tag{27}$$

Substituting (26) into (5)–(7) and retaining leading order linear terms as $\tau \to 0$ yields

$$\mathscr{R}_s + \frac{1}{\xi^2}(\xi^2 \mathscr{U})_\xi = 0 \tag{28}$$

$$\mathscr{U}_s - \frac{1}{3}\mathscr{U} + \frac{2}{3\xi^2}\int_0^\xi \zeta^2 \mathscr{R}(\zeta, s)\, d\zeta = 0 \tag{29}$$

Eliminating $\xi^2\mathscr{U}$ in these equations yields an equation for the growth of the perturbation $\mathscr{Y} = \xi^2\mathscr{R}$,

$$\mathscr{Y}_{ss} - \tfrac{1}{3}\mathscr{Y}_s - \tfrac{2}{3}\mathscr{Y} = 0 \tag{30}$$

Solutions of (30) have exponential growth rates $\lambda = 1, -\frac{2}{3}$, where in terms of physical variables, $\lambda = 1$ corresponds to the unstable perturbations

$$\delta\rho = \tau^{-3}\mathscr{F}(\xi), \qquad \delta u = -\frac{N}{r^2}\int_0^\xi \zeta^2 \mathscr{F}(\zeta)\, d\zeta \tag{31}$$

where $\mathscr{F}(\xi)$ gives the spatial form of the perturbation. Note that this linearized stability analysis yields no constraints on the form of $\mathscr{F}(\xi)$. Hence, at linear order, disturbances of any form can grow on the curves, $\xi = \text{const}$, which correspond to the inward family of characteristics. This wavelike propagation of the perturbations to the uniform core solution reflects the hyperbolic nature of the governing equations. Note that as $\tau \to 0$, the core density grows like $O(\tau^{-2})$ but the perturbation grows at the faster rate $O(\tau^{-3})$ and hence the uniform core solution is unstable.

A simple interpretation of the τ^{-3} growth law is that it corresponds to the perturbation *shifting* the blow up time t_c by a small amount. On changing $t_c \to t_c + \delta$, the maximum density changes from $O((t_c - t)^{-2}) \to O((t_c + \delta - t)^{-2}) = O((t_c - t)^{-2} + \delta(t_c - t)^{-3})$. Spatial nonuniformity is produced when different spatial locations try to collapse at different times.

We now present simulations demonstrating what happens after the instability of the core. Extensive numerical simulations have revealed two different types of qualitative behavior; either the density field remains monotone throughout its evolution, and the solution approaches the same asymptotics seen for $N < N_C$, or the density field becomes nonmonotone, and does something qualitatively different.

First we show an example of monotone collapse at $N = 30$. A one percent random spatial density perturbation is added to the initial gas cloud. Figure 8a shows the density profiles, and Fig. 8b shows the velocity profiles. The behavior follows the uniform core solution up to $\rho \sim 10^6$, after which a transition occurs that leads to the Larson–Penston similarity solution. This is clearly seen in the velocity plot; at late times, the infall velocity asymptotes to the Larson–Penston value of -3.3.

To illustrate the other possible mode of perturbed behavior that we observed, two simulations resulting in nonmonotone density profiles are shown (see Figs. 9 and 10). First, we consider $N = 50$, with a one percent random fluctuation in the initial density. Figure 9 shows that the uniform density core persists until $\rho \sim 10^6$, after which time a nonmonotonicity in the profile develops. Corresponding to the density, the velocity profiles steepens and appears to form an inward propagating shock. The steepness and intensity of the shock appear to be directly related to the magnitude of the nonmonotonicity of the density profile. Further, more sophisticated numerical simulations will be needed to accurately resolve the latter stages of the evolution of this solution.

Unstable nonmonotone density profiles can also be triggered by stochastic forcing in the equations. Figure 10 shows a simulation at $N = 50$,

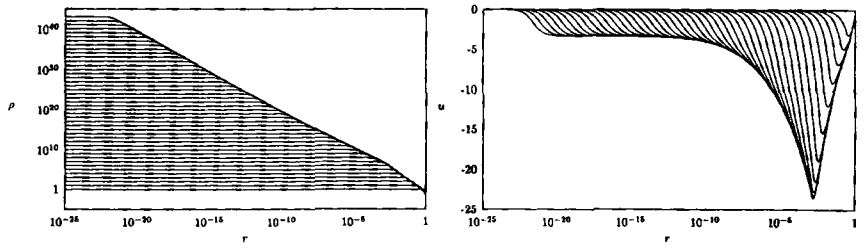

Fig. 8. Convergence to the Larson–Penston solution at $N = 30$ with instabilities to the uniform core solution initiated by small random fluctuations in the initial density profile.

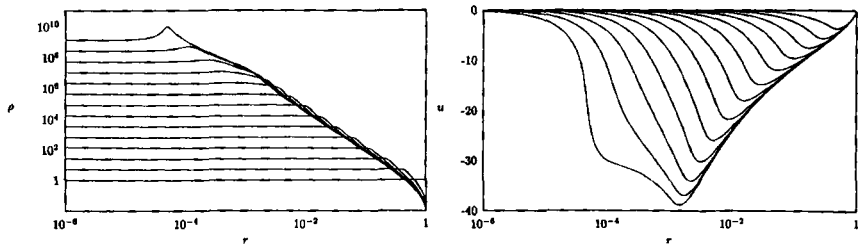

Fig. 9. Formation of a nonmonotone profile at $N = 50$ stimulated by 1% noise in the initial data.

with uniform initial conditions but with small stochastic perturbations added to the momentum equation. The small perturbations yield an instability at $\rho \sim 10^6$, and again a shock-like structure forms in the velocity.

Instabilities in the solution can also arise from various discretization errors in numerical schemes. As will be discussed later, solution of problems that form localized singularities require numerical schemes that allow for highly adaptive spatial grids and time-steps to maintain adequate resolution of the singularity. Figure 7 for $N = 30$ shows that our numerical scheme accurately reproduced the uniform density core solution until $u \approx -400$, when large velocity gradients caused numerical instabilities. Note that this simulation suggests that numerical errors introduced are relatively weak and would begin to effect the structure of the solution well after the instabilities associated with the real perturbations introduced in the earlier simulations.

This section has described some of the behavior observed in simulations of collapse for $N > N_C$ and clearly suggests that the solutions of (1)–(3) are unstable. This is in contrast to the behavior of gravitational collapse for $N < N_C$, where our simulations are independent of any perturbations

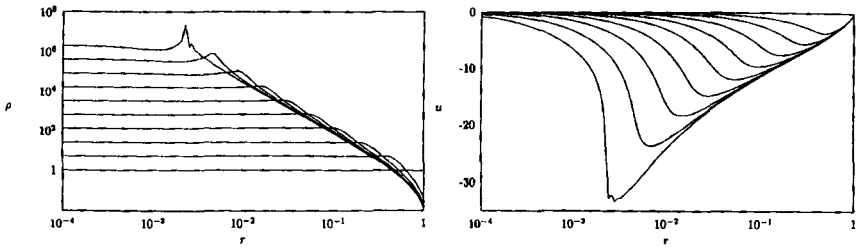

Fig. 10. Formation of a shock at $N = 50$ stimulated by small stochastic forcing in the momentum equation.

added to the system and the solution ultimately converges to the Larson–Penston similarity solution. In the absence of any perturbations, gravitational collapse should be completely described by the uniform density core solution; however this behavior was not expected to be stable. Yet, perturbed solutions do not necessarily show a unique stable nonlinear attracting behavior either, as solutions can settle down to the similarity solution or develop shocks. The addition of perturbations to the solution can be used to approximately incorporate and model the influences of effects not included in the governing equations, for example turbulent flow in the gas cloud. These points suggest that the asymptotic solutions describing gravitational collapse for $N > N_C$ are not universal. The basins of attraction of the two asymptotic solutions found here are very close to each other. We have not been able to find a definitive criterion for determining which solution occurs for given initial data.

4. SELF-SIMILAR SOLUTIONS

The analysis of the preceding section addresses the dynamics during the first regime of the collapse, when the uniform density core collapses. In both the subcritical, $N < N_C$, and supercritical cases, it was argued that this initial regime cannot proceed indefinitely towards the collapse; in the subcritical case, this is because the initial regime only produces a finite density at the origin. In the supercritical case, the dynamics is generically unstable. This section begins to address the question of the final dynamics of the collapse.

The question of the nature of the asymptotic collapse was first addressed by Larson[3] and Penston,[13] who found a self-similar solution of the hydrodynamic equations governing the collapse. Their solution is of the form

$$\rho(r, t) = \frac{1}{N\tau^2} R(\eta, s) \qquad u(r, t) = U(\eta, s) \qquad \phi(r, t) = \frac{1}{N} P(\eta, s) \tag{32}$$

where

$$\tau = t_c - t, \qquad \eta = \frac{r}{\tau}, \qquad s = -\ln(\tau) \tag{33}$$

and as collapse is approached $t \to t_c$, $s \to \infty$. Substituting this ansatz into equations (5)–(7) yields the evolution equations

$$R_s + (U+\eta)\, R_\eta + RU_\eta + \frac{2R}{\eta}(U+\eta) = 0 \tag{34}$$

$$U_s + (U+\eta)\, U_\eta + \frac{R_\eta}{R} - P_\eta = 0 \tag{35}$$

$$P_{\eta\eta} + \frac{2}{\eta} P_\eta + R = 0 \tag{36}$$

Physically, this choice of similarity variables uniquely balances inertia, pressure and gravitational forces. As $\tau \to 0$, the influence of the boundary of the domain is pushed out to $\eta \to \infty$, hence there are no lengthscales in the problem and self-similar dynamics can be expected. The formation of a localized singularity in this system describes a finite-time self-similar blow-up of density in a small neighborhood of the origin. Away from this neighborhood, physical quantities must vary slowly as $t \to t_c$, independent of the fast timescale, s, describing the approach to singularity. This condition yields the asymptotic boundary conditions as η and $r \to \infty$,

$$R = O(\eta^{-2}), \qquad U = O(1), \qquad \eta \to \infty \tag{37}$$

Equations (34)–(37) have steady-profile self-similar solutions that are independent of s; $R = R(\eta)$, $U = U(\eta)$. This type of solution is sometimes called a progressing wave in gas-dynamics.[23] The problem for the self-similar solutions can be reduced to a system of two first order ordinary differential equations. An equation for U_η in terms of U and R can be obtained directly from (34). The gravitational potential $P(\eta)$ can be eliminated from,the remaining equations by noting that (34) and (36) can be combined to produce $P_\eta + R(U+\eta) = 0$, yielding

$$\frac{dU}{d\eta} = \frac{(U+\eta)[2 - \eta R(U+\eta)]}{\eta[(U+\eta)^2 - 1]} \tag{38}$$

$$\frac{dR}{d\eta} = \frac{R(U+\eta)[\eta R - 2(U+\eta)]}{\eta[(U+\eta)^2 - 1]} \tag{39}$$

For $\eta \to \infty$, a two-parameter family of solutions exists with $R \sim R_\infty/\eta^2$ and $U \sim U_\infty$, satisfying boundary conditions (37). These equations have singular points at the origin, $\eta = 0$, and at points satisfying the equation $(U+\eta)^2 = 1$. Expanding about $\eta = 0$, there is a one-parameter family of solutions,

$$R(\eta) \sim R_0 - \frac{(3R_0 - 2)\, R_0}{18}\eta^2, \qquad U(\eta) \sim -\frac{2}{3}\eta + \frac{3R_0 - 2}{135}\eta^3 \tag{40}$$

where $R_0 > 0$ is the scaled self-similar density at the origin. For $R_0 > 2/3$ the radial density profile is monotone decreasing, while for $R_0 < 2/3$ it is locally increasing at the origin. Also note that $R = 2/3$, $U = -2\eta/3$ is an exact, closed-form solution of (38), (39).

In the dilating reference frame defined by the similarity variables (32), the points satisfying $(U+\eta)^2 = 1$ analogous to *sonic points* in transonic flow,[23] where there is a qualitative change in the behavior of the characteristics. This behavior can be seen by writing equations (34)–(36) in characteristic form

$$\frac{dA}{ds} + 2 + \frac{2}{\eta} U - F = 0 \qquad \text{on} \qquad \mathscr{C}_+ : \frac{d\eta}{ds} = U + \eta + 1 \tag{41}$$

$$\frac{dB}{ds} + 2 + \frac{2}{\eta} U + F = 0 \qquad \text{on} \qquad \mathscr{C}_- : \frac{d\eta}{ds} = U + \eta - 1 \tag{42}$$

where the gravitational force F is given by

$$F \equiv p_\eta = -\frac{1}{\eta^2} \int_0^\eta \zeta^2 R(\zeta, s)\, d\zeta \tag{43}$$

and the Riemann variables are

$$A = \ln(R) + U, \qquad B = \ln(R) - U \tag{44}$$

For gravitational collapse, ultimately the velocity everywhere is negative, $U \leqslant 0$, the $\mathscr{C}_+$ characteristics always propagate outward. In contrast, the $\mathscr{C}_-$ characteristics change direction at η_*, where $U(\eta_*) = 1 - \eta_*$, with characteristics for $\eta < \eta_*$ going to the origin, while characteristics for $\eta > \eta_*$ propagating outward. The sonic point creates a separation between an inner region, $0 \leqslant \eta \leqslant \eta_*$, and an outer region of the flow for $\eta > \eta_*$. The information from the inner region can propagate out, but perturbations in the outer region can not effect the inner region. Thus, the details of the similarity solution governing the final collapse is independent of the far-field behavior in the cloud. Note that due to the time-dependent stretching of the spatial coordinates introduced by the similarity variables, the sonic point is not the same as the position that separates supersonic flow, $|u| > 1$ from subsonic flow $|u| < 1$. Indeed, for the initial cloud starting from rest, $u = 0$, the sonic point is $\eta_* = 1$. In general, the position of the sonic point is a function of time $\eta_* = \eta_*(s)$ that must be obtained as part of the solution of a moving boundary problem for the similarity problem. We will briefly discuss some of the details of the properties of stationary solutions

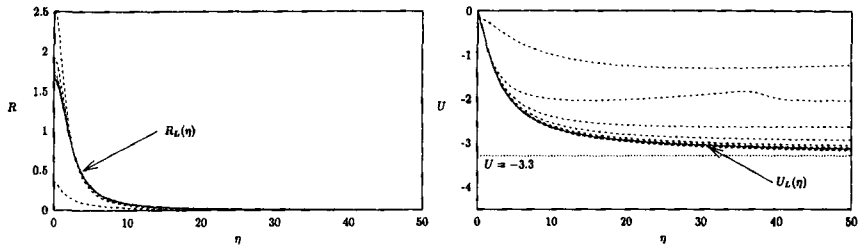

Fig. 11. Convergence of the solution for $N=10$ to the Larson–Penston similarity solution, $R_L(\eta)$, $U_L(\eta)$.

at the sonic point in the appendix. Our numerical simulations suggest that for all $N < N_C$ the dynamics converge to the Larson–Penston solution (see Fig. 11). It is possible that the occurrence of the Larson–Penston solution comes about from a connection between it's unique smoothness properties and spatial discretization characteristics of numerical schemes. On analytical grounds we can not satisfactorily rule out the possibility of other similarity solutions occurring during the dynamics as transient meta-stable states.

It is possible to obtain more insight on the dynamics of collapse by restating the uniform density model in terms of the similarity variables, $R(\eta, s) = \bar{R}(s)$, $U(\eta, s) = \bar{U}(s)\eta$, yielding the autonomous system

$$\frac{d\bar{R}}{ds} = -\bar{R}(2+3\bar{U}), \qquad \frac{d\bar{U}}{ds} = -\frac{\bar{R}}{3} - (\bar{U}+1)\,\bar{U} \tag{45}$$

In this formulation, the phase plane has equilibrium points at $(\bar{R}, \bar{U}) = (0, 0)$, $(0, -1)$ and $(\frac{2}{3}, -\frac{2}{3})$ which is a hyperbolic saddle point (See Fig. 12). The line $\bar{U}=0$, $\bar{R}_0 > 0$ corresponds to the set of initial conditions starting from rest with uniform density. More specifically, the initial value of $\bar{R}$ corresponding to $\rho = 1$ is given in terms of the collapse time t_c as $\bar{R}_0 = Nt_c^2$. The stable branch of the hyperbolic saddle point $(\frac{2}{3}, -\frac{2}{3})$ intersects the line $\bar{U}=0$ at the value $\bar{R}_c = 3\pi^2/8 \approx 3.7$. This value of $\bar{R}$ separates the set of uniform initial conditions into solutions whose density blows up faster than the self-similar solutions and solutions whose scaled density approaches zero. If $\bar{R}_0 = \bar{R}_c$ then the solution approaches the equilibrium steady-profile similarity solution $R = \frac{2}{3}$, $U = -2\eta/3$. Note that the value of the collapse time corresponding to this solution is given by (25). For $\bar{R}_0 < \bar{R}_c$, all solutions approach the zero density fixed point at the origin. This behavior suggests that either (a) no collapse occurs, or (b) the value of t_c that has been used is larger that the real critical time. For $\bar{R}_0 > \bar{R}_c$, the density will initially decrease to a minimum value then increase forever, $\bar{R}(s) \to \infty$

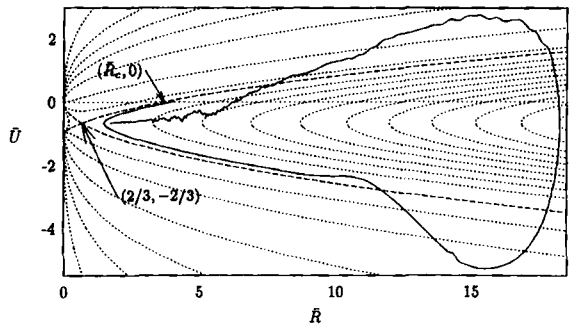

Fig. 12. Plot of the numerical simulation for gravitational collapse at $N = 10$ on the $(\bar{R}, \bar{U})$ plane (solid curve). The positions of the saddle point $(\frac{2}{3}, -\frac{2}{3})$ and the critical initial scaled density $\bar{R}_c = 3\pi^2/8 \approx 3.7$ are shown.

while $U \to -\infty$ in a monotone way. This behavior describes a collapse singularity that blows up faster than the similarity variables. In fact, the eigenvalues of the saddle point are $\lambda = -\frac{2}{3}$ and $\lambda = 1$, so the unstable density solutions actually blows up like $\bar{R} \sim e^s$ or in terms of real variables $\rho \sim (t_c - t)^{-3}$. This behavior is the same as that computed via direct stability analysis in the previous section; its physical interpretation (as an indication of a change in t_c) is therefore identical.

In Fig. 12 we plot the results of the numerical simulation for $N = 10$ on the $(\bar{R}, \bar{U})$ phase plane, where the value of $t_c \approx 0.635461134336$ was obtained from the simulation. We note that $\bar{R}_0 > \bar{R}_c$ and the initial dynamics of the solution follow the uniform core phase plane near the unstable manifold of the saddle point. Eventually, as pressure effects become significant, the solution displays large deviations from the uniform-state trajectories. It should be noted however, that as the final collapse is approached and the solution converges to a self-similar form, the local expansion of the solution about $\eta = 0$ must be given by (40) and hence $\bar{U}(s \to \infty) \to -\frac{2}{3}$ and $\bar{R}(s \to \infty) \to R_0$.

5. NUMERICAL SCHEMES AND SPURIOUS SOLUTIONS

One of the major challenges of this study was to design and evaluate numerical algorithms for accurately computing the high N collapse. The dynamics above N_C is very sensitive, and slight errors in the numerical scheme can lead to large errors in the amount of collapsed mass, as well as the detailed dynamics. Apart from the specific problem of gravitational collapse, precise computation of self-similar singularities is an important feature occurring in many problems in fluid dynamics.[1]

The calculations presented in the previous sections use equations (9) and (10) for the Riemann variables on the characteristic curves to evolve the density and velocity. To sufficiently resolve the solution as the density grows rapidly over decades of magnitude and the lengthscales become exceedingly small it is crucial to use efficient adaptive time-stepping and spatial regridding. Our explicit numerical scheme used Euler time-stepping combined with cubic spline interpolation to project the characteristics back onto the grid points. As spatial structure developed on finer lengthscales, the numerical scheme projects the solution onto a new log-uniformally-spaced grid starting at smaller scales. This method was found to produce sharp, well resolved numerical results that closely matched the uniform core analytic solution (see Fig. 2).

Major pitfalls were encountered in using other numerical schemes which can become underresolved, or which do not respect the hyperbolic nature of the governing equations. An alternative formulation of the problem for (5–7) given in terms of the cumulative mass $m(r, t)$[16] is

$$m_t + um_r = 0 \tag{46}$$

$$u_t + uu_r + \frac{\rho_r}{\rho} + N\frac{m}{r^2} = 0 \tag{47}$$

$$\rho = \frac{m_r}{r^2} \tag{48}$$

These equations were discretized in a standard nonlinear fully-implicit upwind finite-difference method.[35, 36] It is well known that such numerical schemes introduce additional weak dissipative and dispersive influences.[24] The nature of these influences can have a significant impact on the smoothness properties of the numerical solution and ultimately, on the selection of the similarity solution (see the Appendix).

An example using this numerical scheme with $N = 1000$ is shown in Figs. 13 and 14. This simulation was performed with adaptive mesh refinements along the lines of standard algorithms (e.g., Drury and Dorfi[37]). Both the discretization and the regridding introduce perturbations and dispersion into the numerical scheme, when compared with the hyperbolic algorithm used in producing the results of the subsequent sections. The initial dynamics looks much the same those in Section 3 with $N > N_C$: a constant density region is followed by a transition to a monotone density similarity solution. However, there are a few important differences:

First, the destabilization of the constant density region occurs when $\rho \approx 10^6$, and is caused by perturbations induced by the remeshing algorithm, which periodically adjusts the mesh to maintain resolution. In

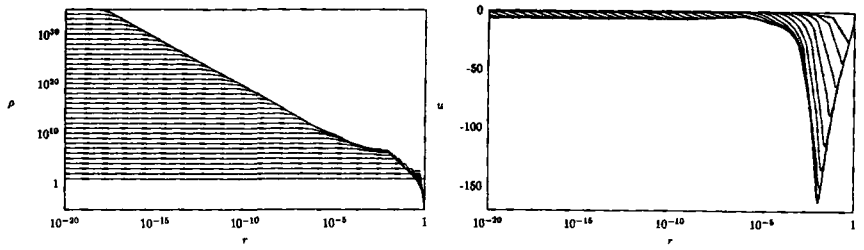

Fig. 13. Evolution of density and velocity fields for $N = 1000$, using a code based on a straightforward discretization of equations (46–48). profiles closer to the singular time have higher central density. The density field obeys the r^{-2} law, and the velocity saturates to a constant near the singularity, as expected from Larson–Penston scaling.

adjusting the mesh, smoothness in both the grid and in the profiles is maintained up to second derivatives (via cubic splines). This behavior is in contrast,to simulations made with the hyperbolic algorithm in Section 3; For example, the simulation in Fig. 8 only shows a transition to the Larson–Penston solution because a perturbation is included to the initial data; without perturbations, the constant-density solution should continue indefinitely.

Secondly, although the asymptotic regime qualitatively looks like it converges to the Larson–Penston localized solution, with $\rho \sim r^{-2}$ law holding in the far field, there is a quantitative discrepancy. In particular, the asymptotic infall velocity near the collapse point is $u \approx -7c$, instead of Larson's value $-3.3c$. Moreover, the solution appears to oscillate around this value as it approaches the singularity. The scale of the oscillation is

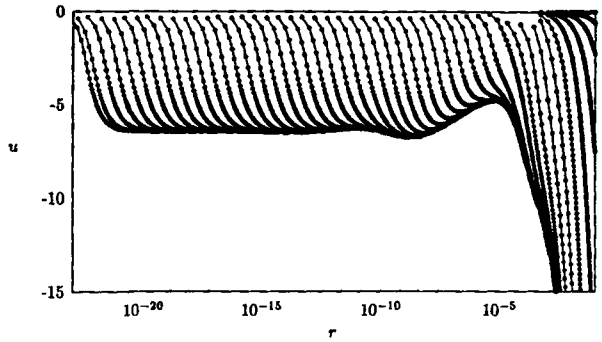

Fig. 14. Blowup of the velocity field near the collapse point. The points represent mesh points in the computation. Note that the velocity asymptotes to a constant away from the collapse point, although the constant differs from the Larson–penston value -3.3. The approach to the constant involves oscillations in space over about five decades.

about five decades of scaling, which is completely unrelated to the remeshing algorithm. This is a serious discrepancy with the Larson–Penston prediction, especially in light of the fact that the asymptotic value of the velocity in the similarity solution is supposed to be universal.

The resolution of a velocity profile in the asymptotic regime is shown in Fig. 14; the density of mesh points appears high. An important point is that in this simulation, the sonic point occurs at about $u \approx -3$. Although outside of the sonic point, the density of points is high, there are only about 10 points inside the sonic point. A priori, it is not clear that this is a problem. However, the code that we used for the simulations in Section 3 only observes convergence to Larson's value of the infall velocity. We therefore believe that the solution depicted in Figs. 13 and 14 might be spurious. Comparing the two codes, there are two possible reasons for this artifact: (a) The code used in Section 3 respects the hyperbolicity of the equations, whereas the code used to produce Figs. 13 and 14 does not. It could be that the spurious dissipation present in this code stabilizes solutions that are unstable otherwise. (b) The low resolution around the sonic point in this simulation could be the source of the problem.

As discussed in the appendix, we believe that the issue is that there is a two parameter family of similarity solutions[38] that have the same qualitative structure as Larson's solution, but with a continuous family of different infall velocities. These additional solutions have discontinuities in derivatives across the sonic point, and are individually unstable, as shown originally by Ori and Piran[39]—and elaborated in the appendix. However, it is unclear that the *family* of solutions does not take part in the dynamics. In principle, it should be possible for a solution to perform an "orbit" in the two parameter space of these additional solutions. We believe that the simulation shown in Fig. 14 may represent such an orbit. The fact that we do not see these solutions in our best simulations lead us to believe that the numerical solutions depicted in the above figures are spurious, and that in actuality the "orbits" in the two parameter family of similarity solutions are unstable. We caution that this is not a rigorous argument but simply our best guess based on the evidence at hand.

The upshot of these problems is that great care is called for if accurate numerical simulations are necessary. These concerns are not only of academic interest for the numerically inclined: if the collapsed mass is defined as the mass contained in some threshold radius, i.e., 10^{-3} times the initial cloud radius, then its value is very sensitive to the noise level and accuracy of the simulations. For example, the amount of collapsed mass contained in Fig. 13 is lower than would exist in a noise free simulation. A corollary to this numerical warning is that physical fluctuations can have a substantial effect on collapsed masses.

6. CONCLUSIONS

The main result of this study is the identification of a nonlinear threshold $N_C = 3\pi^2/2$, above which the dynamics near the collapse point is not universal. In this regime, three different collapse scenarios are possible, depending on (slight) details of the initial data: (a) Collapse with a uniform core, in which (of order) the entire cloud mass collapses to a point; (b) Collapse via the Larson–Penston similarity solution, in which only a small fraction of the total mass participates in the collapse, and the asymptotic velocity near the collapse point is $-3.3c$; (c) An apparently new collapse scenario, in which the density profile becomes increasingly more nonmonotone as the material density diverges, and the velocity profile tends to a shock. For $N < N_C$, only the Larson–Penston scenario is possible. Above N_C, any of (a), (b) or (c) can occur depending on the characteristics of the initial conditions and noise sources.

We have also highlighted numerical difficulties that arise when trying to capture the details of the collapse. Besides standard considerations (i.e., the need for the numerical scheme to respect the hyperbolicity of the equations) we have also found that underresolution can lead to (apparently) spurious numerical solutions. Unless examined very carefully, the solutions all look legitimate. This problem is compounded by the fact that near a singularity, where characteristic scales are vanishingly small, a simulation that looks well resolved in real space could be insufficiently resolved when scaled in terms of the characteristic collapsing lengthscale. For a reason that might be very specific to this particular problem, (the existence of a continuous family of similarity solutions that our numerical simulations indicate is apparently unstable), maintaining high resolution in similarity variables turned out to be crucial.

It is notable that this difficulty occurs in a problem which is relatively simple, involving only one spatial degree of freedom. Questions of actual astrophysical interest (e.g., Boss's[5] simulations on giant planet formation mentioned in the introduction) require understanding the collapse dynamics in three spatial dimensions. Since three-dimensional simulations necessarily have far less resolution than the present study (e.g., Boss's simulations take place on a 51 by 23 by 64 mesh), the difficulties reported here could occur in these contexts as well. It is not clear how errors in resolving the detailed collapse dynamics translate into errors in observable quantities like the mass or angular momentum of a protostar. An important direction for future research is to develop analytical and theoretical tests for answering these questions, both with regards to the numerical algorithms, and to the hyperbolic equations themselves. Perhaps the development of such ideas in the context of one dimensional models will help improve and evaluate the accuracy of larger scale simulations.

The relevance of the present results for problems of astrophysical interest has some limitations. These are at least two types of complications: First, the assumption of isothermal dynamics is a dramatic idealization, and will at best only apply over a finite number of decades of increasing material density. Some of the features uncovered in this study require several decades of scaling to develop. The complications to isothermal gas dynamics include heat and radiation transfer, the influence of magnetic fields, and many other factors.[9, 11] Perhaps an even more significant assumption is the restriction to spherically symmetric collapse, with zero angular momentum. In this regard, this work has the same deficiency as the original studies of Larson. Both Shu[14] and Larson[40, 41] have emphasized that the determination of the relevant mass of the collapsing spherical object (or alternatively, the relevant parameter N) depends on the mechanisms for clumping in the fully three-dimensional dynamics. Larson[41] has suggested an intriguing connection between the masses of clumps, and the geometrical structures from which they form. From this viewpoint, a conclusion of the present study is that the qualitative dynamics of the final collapse is sensitive to the mass of the collapsing object, and hence the geometrical structures forming in fully three-dimensional collapse.

Finally, from the perspective of the general problem of singularity formation in nonlinear partial differential equations, the present study appears to have the novel feature that above a critical threshold N_C in initial data, the asymptotic collapse state is not universal. Three different possible asymptotic states have been given (one of which was previously identified). Very slight changes in initial data can lead to transitions between the different asymptotic states. We do not know whether this property is a peculiarity of the present problem, or is a general property of dissipation/dispersionless singularity formation.

APPENDIX A: SOLUTIONS OF THE SIMILARITY EQUATIONS

The goal of this appendix is to describe additional properties of the similarity equation, which are important for understanding and interpreting results of numerical experiments. It turns out that there is an additional *two parameter* family of the similarity equations, discovered originally by Wentworth and Summers,[38] which were previously argued to be unstable.[39] Herein, we present our own derivation and interpretations of these additional solutions. We demonstrate that these solutions have the peculiar property of having discontinuities in higher derivatives at the sonic point. (The order of the discontinuity can be made arbitrarily high by moving about in the two parameter family). The upshot of our discussion is that although we agree with previous authors that these solutions exist and that

they are individually unstable, the stability arguments do not rule out orbits in the two parameter family of additional solutions. These orbits would be characterized by different asymptotic values of the parameters (i.e., velocity far from the collapse point). One set of our numerical simulations (described in Section 5) displays solutions which appear to resemble these orbits; for the reasons discussed therein we believe these are spurious numerical solutions. However, we are not able to rule out the existence of such solutions in numerical simulations and hence it is possible that our description of the dynamics for $N > N_C$ is an oversimplification.

We now proceed to derive the additional solutions. As stated above, our discussion is in the same spirit as Wentworth and Summers,[38] though the argument appears more straightforward. The sonic point η_* of a solution is a movable singular point of (38), (39) defined by $U(\eta_*)+\eta_*=1$. Analysis of the local expansion around I* yields important information about the structure of the set of similarity solutions. Requiring η_* to be a removable singularity yields two possible analytic Taylor series expansions, denoted type-1[16, 14]

$$U_1(\eta) \sim (1-\eta_*) + \left(\frac{1}{\eta_*} - 1\right)(\eta-\eta_*) + \frac{\eta_*-1}{2\eta_*^2}(\eta-\eta_*)^2 \tag{A1}$$

$$R_1(\eta) \sim \frac{2}{\eta_*} + \frac{2}{\eta_*}\left(1-\frac{3}{\eta_*}\right)(\eta-\eta_*) + \frac{\eta_*^2-8\eta_*+13}{\eta_*^3}(\eta-\eta_*)^3 \tag{A2}$$

and type-2,

$$U_2(\eta) \sim (1-\eta_*) - \frac{1}{\eta_*}(\eta-\eta_*) - \frac{5-5\eta_*+\eta_*^2}{2\eta_*^2(2\eta_*-3)}(\eta-\eta_*)^2 \tag{A3}$$

$$R_2(\eta) \sim \frac{2}{\eta_*} - \frac{2}{\eta_*^2}(\eta-\eta_*) - \frac{7-6\eta_*+\eta_*^2}{\eta_*^3(2\eta_*-3)}(\eta-\eta_*)^2 \tag{A4}$$

Any possible smooth solutions must have one these two local forms. Global solutions must additionally satisfy the boundary conditions at the origin $\eta=0$ (40). The Larson–Penston solution is a type-2 solution with $\eta_* \approx 2.34$, while the closed-form exact solution, $R=\frac{2}{3}$, $U=-2\eta/3$, is a type-1 solution with $\eta_*=3$.

Simple counting arguments would then imply that there is a unique (or at most, a countable) set of solutions connecting the origin to the sonic point (since naively one condition is specified at each location), so that there should be (at most) a countable set of solutions to the similarity equations. This type of reasoning originally led Larson to find his solution

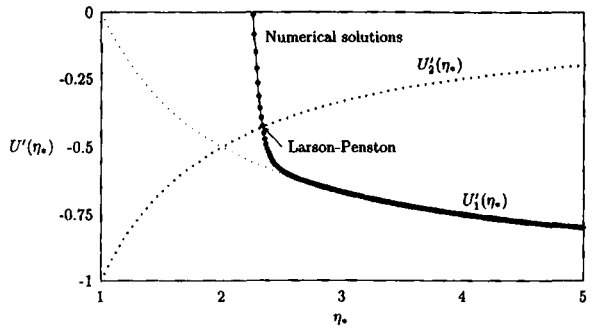

Fig. 15. A continuous family of inner similarity solutions on $0 \leqslant \eta \leqslant \eta_*$ parametrized by $(\eta_*, U'(\eta_*))$. The numerical solutions are compared with $U'(\eta_*)$ for the type-1, $U_1'(\eta_*) = 1/\eta_* - 1$, and type-2, $U_2'(\eta_*) = -1/\eta_*$ analytic solutions. The Larson–Penston solution with $\eta_* \approx 2.34$ is the unique type-2 solution found here.

(see Fig. 11). In fact, the position of the sonic point serves to decouple the problem into two intervals; an inner solution for $0 \leqslant \eta \leqslant \eta_*$, and an outer solution for $\eta_* < \eta < \infty$. Numerical solution of the inner problem shows that while Larson's solution is the unique smooth type-2 solution, there is a continuous family of solutions parametrized the sonic point for all $\eta_* > 2$ (see Fig. 15).

It turns out that the situation is more complicated than a simple counting argument would suggest, a fact that was first appreciated by Whitworth and Summers.[38] The reason for this can be seen by writing the equations near the sonic point as an autonomous system and then considering the linear stability in the neighborhood of η_*. To do this we must introduce a change of variables that converts the sonic point from a removable singularity of the equations to an equilibrium point.[42] Let

$$U = U(\zeta), \qquad R = R(\zeta), \qquad \eta = \eta(\zeta) \tag{A5}$$

where the change of variables is defined by

$$\frac{dU}{d\zeta} = \frac{(U+\eta)[2 - \eta R(U+\eta)]}{\eta(U+\eta+1)} \tag{A6}$$

$$\frac{dR}{d\zeta} = \frac{R(U+\eta)[\eta R - 2(U+\eta)]}{\eta(U+\eta+1)} \tag{A7}$$

$$\frac{d\eta}{d\zeta} = U + \eta - 1 \tag{A8}$$

This third order system has the one-parameter continuous family of equilibrium points,

$$\mathbf{x}_*^T = (U_* \quad R_* \quad \eta_*) = (1-\eta_* \quad 2/\eta_* \quad \eta_*) \tag{A9}$$

for any choice of $\eta_* > 0$. The Jacobian matrix for the linearization about this equilibrium point is

$$\mathbf{J}_* = \begin{pmatrix} -\dfrac{1}{\eta_*} & -\dfrac{1}{2} & -\dfrac{1+\eta_*}{\eta_*^2} \\ -\dfrac{2}{\eta_*^2} & \dfrac{1}{\eta_*} & \dfrac{2-2\eta_*}{\eta_*^3} \\ 1 & 0 & 1 \end{pmatrix} \tag{A10}$$

The eigenmodes for the system $\mathbf{J}_*\tilde{\mathbf{x}} = \lambda\tilde{\mathbf{x}}$, for any η_* are given by;

1. A zero eigenvalue that corresponds to the continuous symmetry of picking a different sonic point, $\eta_* \to \eta_* + \varepsilon$,

$$U \to 1-\eta_*-\varepsilon \qquad R \to \frac{2}{\eta_*} - \frac{2}{\eta_*^2}\varepsilon \qquad \eta_* \to \eta_* + \varepsilon \tag{A11}$$

yielding the linearized eigenmode

$$\lambda = 0 \qquad \tilde{\mathbf{x}}_*^T = \left(-1 \quad -\frac{2}{\eta_*^2} \quad 1\right) \tag{A12}$$

2. An eigenmode corresponding to the U_1, R_1 solution

$$\lambda_1 = \frac{1}{\eta_*} > 0 \qquad \tilde{\mathbf{x}}_1^T = \left(\frac{1-\eta_*}{\eta_*} \quad \frac{2(\eta_*-3)}{\eta_*^2} \quad 1\right) \tag{A13}$$

3. An eigenmode corresponding to the U_2, R_2 solution

$$\lambda_2 = \frac{\eta_*-1}{\eta_*} > 0 \qquad \tilde{\mathbf{x}}_2^T = \left(-\frac{1}{\eta_*} \quad -\frac{2}{\eta_*^2} \quad 1\right) \tag{A14}$$

For $\eta_* > 1$, both $\lambda_2 > 0$, $\lambda_1 > 0$ and the sonic point is an unstable node with a continuum of solutions connecting to it (see Fig. 16). For $\eta_* > 2$, $\lambda_2 > \lambda_1$, the set of solutions going through η_* can be written as

$$\begin{pmatrix} U \\ R \\ \eta \end{pmatrix} = \mathbf{x}_* + A_2^{\pm} \tilde{\mathbf{x}}_2 e^{\lambda_2 \zeta} + A_1^{\pm} \tilde{\mathbf{x}}_1 e^{\lambda_1 \zeta} \tag{A15}$$

Specifically, we can write the parametric solution

$$\begin{aligned} U(z) &= 1 - \eta_* + A_1^{\pm} \frac{1-\eta_*}{\eta_*} z - A_2^{\pm} \frac{1}{\eta_*} z^k \\ \eta(z) &= \eta_* + A_1^{\pm} z + A_2^{\pm} z^k \end{aligned} \tag{A16}$$

where

$$z = e^{\lambda_1 \zeta}, \qquad k = \frac{\lambda_2}{\lambda_1} = \eta_* - 1 > 1 \tag{A17}$$

Suppose A_2^+, A_1^+ define a right-solution for $\eta \geqslant \eta_*$ and A_2^-, A_1^- define a left-solution for $\eta \leqslant \eta_*$, then equation (A16) defines a solution $U(\eta)$ that has k continuous derivatives at the sonic point.

To determine whether these solutions will be observed it is necessary to determine their stability. Using the linear stability analysis of Hanawa and Nakayama[43] for solutions on $0 \leqslant \eta \leqslant \eta_*$, it can be shown that all of the solutions should be stable. A different approach, considered by Ori

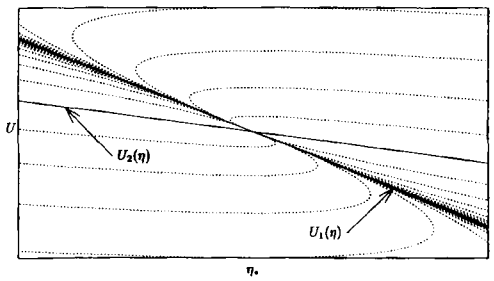

Fig. 16. Local structure of the family of $U(\eta)$ solutions near the sonic point η_*. The analytic solutions $U_1(\eta)$ and $U_2(\eta)$ are the slow and fast manifolds going into the stable node $(\eta_*, U(\eta_*))$. Physically relevant single-valued solutions lie in the sector bounded by $U_1(\eta)$ and $U_2(\eta)$.

and Piran,[39] focuses on the local structure of the solutions at the sonic point η_*. They argued that jumps in the first derivative should grow for the extra family of solutions, and hence that they are unstable. Here, we present a refinement of their argument, with a different interpretation of the results. Apart from the type-1 and type-2 solutions, all of the solutions constructed above lose continuity in derivatives at η_* at some order. However, the sonic point defines a characteristic curve of the hyperbolic system (34), (35) and weak solutions satisfying appropriate jump conditions across the characteristic can exist. Carrying out a wavefront expansion[20] on the $\mathscr{C}_-$ characteristic at the sonic point shows that the n-th derivatives must satisfy

$$\begin{bmatrix} U_*^{(n)} \\ R_*^{(n)} \end{bmatrix} = \sigma_n \begin{pmatrix} 1 \\ R(\eta_*) \end{pmatrix} \tag{A18}$$

where $\sigma_n = \sigma_n(s)$ is the jump magnitude and the jump in X across η_* is defined as $[X_*] = X(\eta_*^+) - X(\eta_*^-)$. For $\sigma_n \to 0$, the jump magnitude evolves according to

$$\frac{d\sigma_n}{ds} \sim -\left(n + (n+1)\, U'_* - \frac{1}{2\eta_*} \frac{d\eta_*}{ds} \right) \sigma_n \tag{A19}$$

for $n = 1, 2, \ldots$. This formula agrees with the result derived by Ori and Piran via a more formal argument,[39] except in one important respect: since we are testing the stability of a continuous family of solutions, we have allowed η_* to vary with time, which corresponds to a continuous symmetry in the family of solutions (A11).

Without allowing for variations in η_*, equation (A19) for $n = 1$ predicts instability if $U'(\eta_*) < -\frac{1}{2}$, and stability otherwise. This condition, given by Ori and Piran, implies that all type-1 similarity solutions are unstable. However, if the variation of η_* evolves appropriately (i.e., $d\eta_*/ds = 2\eta_*(1 + 2U'_*)$) stability at the sonic point is maintained, at the expense of the time evolution moving around the family of type-1 solutions. Precisely how this time evolution plays out requires coupling the evolution of η_* to that of $U(\eta \to \infty) = U_\infty$, that is, the outer portion of the similarity solution. Our most highly resolved numerical simulations do not observe evolution on this family, so our evidence evidence is against evolution in this family being stable. However, we emphasize that we cannot rule out that artificial dissipation or dispersion in the numerical scheme causes these solutions to (artificially) destabilize. We also remark that the simulations presented in Section 5 using a different (but, we believe, less reliable) scheme resemble evolution in this continuous family, with the asymptotic velocity U_∞ oscillating in space and time as the singularity is reached.

ACKNOWLEDGMENT

We thank Meredith Betterton, Elena Budrene, Peter Constantin, Jens Eggers, Ruben Rosales, Leonid Levitov, and Shankar Venkaratamani for various types of help. We are especially grateful to Michael Kiessling for both his careful review of the manuscript, and for bringing to our attention Emden's remarkable 1907 book.[25] Support from the NSF Division of Mathematical Sciences (M.B. and T.W.) and the A. P. Sloan Foundation (M.B.) is gratefully acknowledged.

REFERENCES

1. Russel E. Caflisch and George C. Papanicolaou, *Singularities in Fluids, Plasmas, and Optics*, Volume C404 of NATO ASI Series (Kluwer Academic Publishers, 1993).
2. Peter Constantin, Todd F. Dupont, Raymond E. Goldstein, Leo P. Kadanoff, Michael Shelley, and Su-Min Zhou, Droplet breakup in a model of the Hele-Shaw cell, *Phys. Rev. E* **47**:4169–4181 (1993).
3. R. B. Larson, Numerical calculations of the dynamics of a collapsing protostar, *Mon. Not. R. Astr. Soc.* **145**:271–295 (1969).
4. A. J. Majda, Vorticity and the mathematical theory of incompressible fluid flow, *Comm. Pure Appl. Math.* **39**:5187–5220 (1986).
5. A. P. Boss, Giant planet formation by gravititational instability, *Science* **276**:1836 (1997).
6. G. P. Kuiper, On the origin of the solar system, *Proc. Natl. Acad. Sci.* **37**(1):1–14 (1951).
7. M. Mayor and D. Queloz, *Nature* **378**:355 (1995).
8. H. Mizuno, Formation of giant planets, *Prog. Theor. Phys.* **64**:544 (1980).
9. D. C. Black and M. S. Matthews, *Protostars and Planets* (The University of Arizona Press, Tucson, Arizona, 1985).
10. C. J. Lada and N. D. Kylafis, *The Physics of Star Formation and Early Stellar Evolution* (Kluwer Academic Publishers, Boston, 1991).
11. R. Capuzzo-Dolcetta, C. Chiosi, and A. Di Fazio, *Physical Processes in Fragmentation and Star Formation* (Kluwer Academic Publishers, Boston, 1990).
12. M. K.-H. Kiessling, On the equilibrium statistical mechanics of isothermal classical selfgravitating matter, *J. Stat. Phys.* **55**:203–57 (1989).
13. M. V. Penston, Dynamics of self-gravitating gaseous spheres III, *Mon. Not. R. Astr. Soc.* **144**:425–448 (1969).
14. Frank H. Shu, Self-similar collapse of isothermal spheres and star formation, *Astrophys. J.* **214**:488–497 (1977).
15. F. H. Shu, F. C. Adams, and S. Lizano. *Ann. Rev. Astron. Astrop.* **25**:23 (1987).
16. C. Hunter, The collapse of unstable isothermal spheres, *Astrophys. J.* **218**:834–845 (1977).
17. P. N. Foster and R. A. Chevalier, Gravitational collapse of an isothermal sphere, *Astrophys. J.* **416**:303–311 (1993).
18. J. H. Jeans, *Astronomy and Cosmogony* (Cambridge University Press, New York, 1929) (reprinted by Dover, 1961),
19. M. H. Heyer, F. J. Vrba, R. L. Snell, F. P. Schloerb, S. E. Strom, P. F. Goldsmith, and K. M. Strom, *Astrophys. J.* **324**:311 (1987).
20. G. B. Whitham, *Linear and Nonlinear Waves* (Wiley-Interscience, New York, 1974).
21. L. I. Sedov, *Similarity and Dimensional Methods in Mechanics*, 10th ed. (CRC Press, Boca Raton, 1993).

22. Ya. B. Zeldovich and Yu P. Raizer, *Elements of Gasdynamics and Classical Theory of Shock Waves* (Academic Press, New York, 1968).
23. R. Courant and K. O. Friedirchs, *Supersonic Flow and Shock Waves* (Interscience Publisher, New York, 1948).
24. R. J. LeVeque, *Numerical Methods for Conservation Laws* (Birkhauser, Basel, 1992).
25. R. Emden, *Gaskugeln—Anwendungen der Mechan. Warmtheorie* (Druck und Verlag Von B. G. Teubner, Leipzig, 1907).
26. S. Chandrasekhar, *An Introduction to the Study of Stellar Structure* (Dover, New York, 1967).
27. H. T. Davis. *Introduction to Nonlinear Differential and Integral Equations* (Dover, New York, 1962).
28. P. Natarajan and D. Lynden-Bell, An analytic approximation to the isothermal sphere, *Mon. Not. R. Astr. Soc.* **286**:268–270 (1997).
29. F. K. Liu, Polytropic gas spheres: An approximate analytic solution of the lane-emden equation, *Mon. Not. R. Astr. Soc.* **281**:1197–1205 (1996).
30. M. P. Brenner, L. Levitov, and E. O. Budrene, Physical mechanisms for chemotactic pattern formation by bacteria, *Biophys. J.* (1998), to appear, April.
31. M. P. Brenner, P. Constantin, L. P. Kadanoff, A. Schenkel, and S. Venkataramani, Diffusion, attraction, collapse, preprint, 1998.
32. M. Kiessling, private communication.
33. D. Lynden-Bell and Wood, *Mon. Not. R. Astr. Soc.* **138**:495–525 (1968).
34. G. Horwitz and J. Katz. Steepest descent technique and stellar equilibrium statistical mechanics, III. Stability of various ensembles. *Astrophys. J.* **222**:941–958 (1978).
35. H. B. Keller, *Numerical Solution of Two Point Boundary Value Problems* (SIAM, Philadelphia, 1976).
36. R. D. Richtmyer and K. W. Morton, *Difference Methods for Initial-Value Problems* (John Wiley-Interscience, New York, 1967).
37. E. A. Dorfi and L. O'C. Drury, Simple adaptive grids for 1-d initial value problems, *J. Comp. Phys.* **69**:175–195 (1987).
38. A. Whitworth and D. Summers, Self-similar condensation of spherically symmetric self-gravitating isothermal gas clouds, *Mon. Not. R. Astr. Soc.* **214**:1–25 (1985).
39. A. Ori and T. Piran, A simple stability criterion for isothermal spherical self-similar flow, *Mon. Not. R. Astr. Soc.* **234**:821–829 (1988).
40. R. B. Larson, Cloud fragmentation and stellar masses, *Mon. Not. R. Astr. Soc.* **214**:379–398 (1985).
41. R. B. Larson, Towards understanding the stellar initial mass function, *Mon. Not. R. Astr. Soc.* **256**:641–646 (1992).
42. O. I. Bogoyavlensky, *Methods in the ualitative Theory of Dynamical Systems in Astrophysics and Gas Dynamics* (Springer-Verlag, Berlin, 1985).
43. T. Hanawa and K. Nakayama, Stability of similarity solutions for a gravitationally contracting isothermal sphere: Convergence to the Larson–Penston solution, *Astrophys. J.* **484**:238–244 (1997).